Strong Cooperativeness in the Mononuclear Iron(II) Derivative Exhibiting an Abrupt Spin Transition above 400 K

R. Boča,*,† M. Boča,† L. Dlháň,† K. Falk,‡ H. Fuess,‡ W. Haase,‡ R. Jaroščiak,† B. Papánková,† F. Renz,# M. Vrbová,† and R. Werner‡

Department of Inorganic Chemistry, Slovak Technical University, SK-812 37 Bratislava, Slovakia, Institute of Physical Chemistry, Institute of Material Science, Darmstadt University of Technology, D-64289 Darmstadt, Germany, and Institute of Inorganic and Analytical Chemistry, Johannes Gutenberg-University, D-55099 Mainz, Germany

Received July 18, 2000

The spin crossover system, $[Fe(bzimpy)_2](ClO_4)_2 \cdot 0.25H_2O$, was reinvestigated above room temperature (bzimpy = 2,6-bis(benzimidazol-2-yl)pyridine). The system exhibits an abrupt low-spin to high-spin transition at T_c = 403 K. Liberation of a fractional amount of water does not affect the spin crossover: the system is perfectly reversible with a hysteresis width of $\Delta T = 12$ K. The existence of the hysteresis at such high temperature determines that the lowest limit of the solid-state cooperativity parameter is $J/k > 403$ K despite long iron(II) separations (10 Å). The high cooperativeness has been assigned to a perfect π-stacking of the benzimidazole rings in the crystal lattice at a distance as short as 3.6 Å. Variable-temperature IR data and the heat capacity measurements match well the magnetic data. The thermodynamic properties are $\Delta H = 17$ kJ mol^{-1}, $\Delta S = 43$ J K^{-1} mol^{-1}, so that the entropy of the spin transition shows a considerable contribution from the molecular vibrations. A theoretical model has been applied in fitting the magnetic data along the whole hysteresis path. A statistical distribution of the cooperativity parameter led to the feature that angled walls of the hysteresis loop are well reproduced.

Introduction

The spin crossover phenomenon (the low-spin to high-spin transition) is well documented for mononuclear d^4 to d^7 metal complexes; it dominates just for d^6 Fe(II) species.[1] Spin crossover has also been confirmed recently in oligonuclear complexes.[2] The spin transition can be monitored by several experimental techniques such as magnetic susceptibility measurements, calorimetry, Mössbauer spectra, X-ray diffraction, nuclear magnetic resonance, volumetry, vibrational spectra, electron spin resonance, and optical spectroscopy.

The potential application of spin crossover systems for data storage and imaging has been emphasized by several reports.[3] One of the prerequisites, however, is the existence of a transition temperature from low-spin to high-spin state, T_c, near or above room temperature. This limit has been reached for the first time by Larionov et al.[4] using triazole ligands and then reinvestigated and extended to other systems by several groups.[5] Recently an exceptionally abrupt spin transition has been observed and discussed in terms of a π-stacking of aromatic rings.[6]

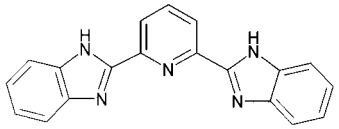

Figure 1. A sketch of the tridentate bzimpy ligand.

We reported previously about the complexes of the type $[Fe(bzimpy)_2]X_2 \cdot nH_2O$ that they exhibit the spin crossover at temperatures as high as $T_c = 330$ K, the organic ligand being bzimpy = 2,6-bis(benzimidazol-2-yl)pyridine—see Figure 1.[7,8]

* To whom correspondence should be sent.
† Slovak Technical University.
‡ Darmstadt University of Technology.
# Johannes Gutenberg-University.

(1) (a) Goodwin, H. A. *Coord. Chem. Rev.* **1976**, *18*, 293. (b) Gütlich, P. *Struct. Bonding* **1981**, *44*, 83. (c) Beattie, J. K. *Adv. Inorg. Chem.* **1988**, *32*, 1. (d) Toftlund, H. *Coord. Chem. Rev.* **1989**, *94*, 67. (e) König, E. *Struct. Bonding* **1991**, *76*, 51. (f) Gütlich, P.; Hauser, A.; Spiering, H. *Angew. Chem.* **1994**, *106*, 2109. (g) Kahn, O. *Molecular Magnetism*; VCH Publishers: New York, 1993. (h) Boča, R. *Theoretical Foundations of Molecular Magnetism*; Elsevier: Amsterdam, 1999.

(2) (a) Real, J. A.; Bolvin, H.; Bousseksou, A.; Dworkin, A.; Kahn, O.; Varret, F.; Zarembowitch, J. *J. Am. Chem. Soc.* **1992**, *114*, 4650. (b) Vos, G.; de Graaff, R. A. G.; Haasnoot, J. G.; van der Kraan, A. M.; de Vaal, P.; Reedijk, J. *Inorg. Chem.* **1984**, *23*, 2905. (c) Breuning, E.; Ruben, M.; Lehn, J.-M.; Renz, F.; Garcia, Y.; Ksenofontov, V.; Gütlich, P.; Wegelius, E.; Rissanen K. *Angew. Chem., Int. Ed.* **2000**, *39*, 2504.

(3) (a) Kahn, O.; Kröber, J.; Jay, C. *Adv. Mater.* **1992**, *4*, 718. (b) Gatteschi, D. *Adv. Mater.* **1994**, *6*, 635. (c) Kahn, O.; Martinez, C. J. *Science* **1998**, *279*, 44.

(4) (a) Lavrenova, L. G.; Ikorskii, N. V.; Varnek, V. A.; Oglezneva, I. M.; Larionov, S. V. *Koord. Khim.* **1986**, *12*, 207. (b) Lavrenova, L. G.; Ikorskii, N. V.; Varnek, V. A.; Oglezneva, I. M.; Larionov, S. V. *Koord. Khim.* **1990**, *16*, 654. (c) Lavrenova, L. G.; Ikorskii, N. V.; Varnek, V. A.; Oglezneva, I. M.; Larionov, S. V. *Polyhedron* **1995**, *14*, 1333.

(5) (a) Vreugdenhil, W.; van Diemen, J. H.; de Graff, R. A. G.; Haasnoot, J. G.; Reedijk, J.; van der Kraan, A. M.; Kahn, O.; Zarembowitch, J. *Polyhedron* **1990**, *9*, 2971. (b) Kröber, J.; Audiere, J. P.; Claude, R.; Codjovi, E.; Kahn, O.; Haasnoot, J. G.; Groliere, F.; Jay, C.; Bousseksou, A.; Linares, J.; Varret, F.; Gonthier-Vassal, A. *Chem. Mater.* **1994**, *6*, 1404.

(6) (a) Letard, J.-F.; Guionneau, P.; Rabardel, L.; Howard, J. A. K.; Goeta, A. E.; Chasseau, D.; Kahn, O. *Inorg. Chem.* **1998**, *37*, 4432. (b) Guionneau, P.; Letard, J.-F.; Yufit, D. S.; Chasseau, D.; Bravic, G.; Goeta, A. E.; Howard, J. A. K.; Kahn, O. *J. Mater. Chem.* **1999**, *9*, 985.

(7) Boča, R.; Baran, P.; Boča, M.; Dlháň, L'.; Fuess, H.; Haase, W.; Linert, W.; Papánková. B.; Werner, R. *Inorg. Chim. Acta* **1998**, *278*, 190.

(8) Boča, R.; Baran, P.; Dlháň, L'.; Fuess, H.; Haase, W.; Renz, F.; Linert, W.; Svoboda, I.; Werner, R. *Inorg. Chim. Acta* **1997**, *260*, 129.

10.1021/ic000807s CCC: $20.00 © 2001 American Chemical Society
Published on Web 05/19/2001

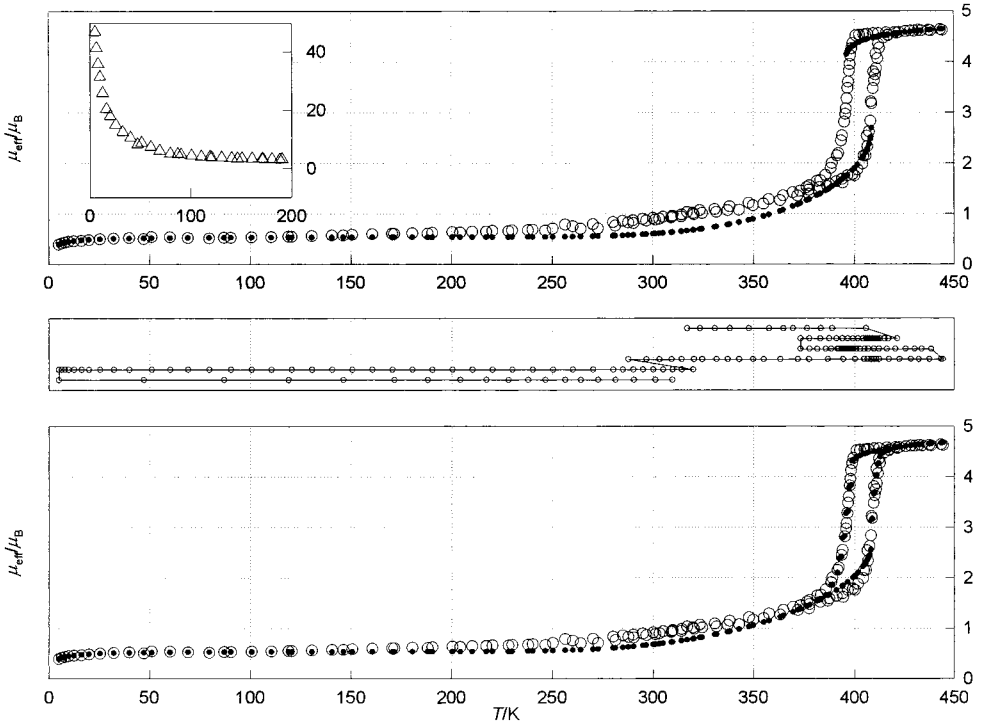

Figure 2. Experimental (open circles) and theoretical (full points, model **A**) data on the effective magnetic moment for **1**. Inset: low-temperature behavior of the magnetic susceptibility. Center: history of the sample cooling/heating. Bottom: model **C**.

The complex having the tetraphenylborate as a counterion, X = BPh_4 and $n = 4$, behaves quite normally: the spin crossover proceeds in one step and the saturation value of the effective magnetic moment is $\mu_{eff} \approx 5.5\ \mu_B$ at $T_{HS} \approx 400$ K.[7] This result implies a magnetogyric factor, $g = 2.54$, being somewhat higher than the free-electron value. The spin transition, however, is rather continuous in this compound and it proceeds within the interval of about 100 K. At temperatures as high as 400 K the complex liberates the crystal water and turns irreversibly to the high-spin species, which remains high-spin on decreasing temperature. On moderate thermal treatment (up to $T = 350$ K) the spin transition is reversible, although incomplete.

The complex with perchlorate as counterion, X = ClO_4 and $n = 0.25$ (the fractional content of water confirmed by X-ray structure analysis),[8] showed saturation features at $T_{HS} \approx 400$ K with $\mu_{eff} \approx 3.5\ \mu_B$. The spin transition seems to be centered at $T_c = 330$ K. A further thermal treatment using DTA showed an endothermic peak at ca. $T_p = 400$ K which we have assigned to the liberation of the crystal water. Attempts to apply the two-level Ising-like model in fitting the experimental data led to a rather problematic result: $g = 1.5$ resulted as an effect of the sub-spin only value of the magnetic moment. The magnetic susceptibility data (taken up to 400 K) were not fully consistent with the VT-IR data (taken up to 520 K): the latter showing a continuation of the spin crossover above 400 K.[9]

The above discrepancies led us to reinvestigate the behavior of the perchlorate complex, $[Fe(bzimpy)_2](ClO_4)_2 \cdot 0.25H_2O$, hereafter **1**, above room temperature. For a freshly prepared microcrystalline sample we applied differential scanning calorimetry to monitor heat flow and to determine the thermal variation of the heat capacity, from which the enthalpy and entropy of the spin transition result. Simultaneously we applied the Faraday balance measurements of the magnetic susceptibility until 443 K. The spin crossover manifests itself in VT IR data as well as in the VT powder diffraction data. Finally we applied an Ising-like model in several variants to fit the magnetic data and to compare the thermodynamic data (enthalpy and entropy of the spin transition) with the direct calorimetric measurements. Now the properties of three samples can be compared: **c**, the freshly prepared microcrystalline sample; **b**, the sample grained to a fine powder; and **a**, a half year old, powdered sample.

Results

The key information about the spin crossover in **1** (sample **c**) is given by the temperature dependence of the magnetic susceptibility (Figure 2).

The effective magnetic moment $\mu_{eff} \approx 0.5\ \mu_B$ below 200 K indicates a presence of a paramagnetic impurity (PI). This is the only source of the paramagnetism at low temperature. The nature of the PI has been assigned to Fe(III) centers on the basis of the ESR signal at 77 K.

On heating above 200 K the effective magnetic moment increases continuously and adopts a value of $\mu_{eff} \approx 1.7\ \mu_B$ at 400 K. On further heating an abrupt spin crossover (within a few K) applies: $\mu_{eff} \approx 4.5\ \mu_B$ at 417 K. A subsequent temperature increase until 443 raises the effective magnetic moment only slightly. (A further heating is risky because of the possible explosion of perchlorate.) On the cooling direction a hysteresis occurs: the magnetic moment stays $\mu_{eff} \approx 4.5\ \mu_B$ at 400 K and then decays abruptly so that $\mu_{eff} \approx 2.0\ \mu_B$ at 390 K.

A further cycling of the sample confirms a perfect reproducibility of all features of the spin crossover (transition onset temperature, abruptness, saturation value, hysteresis width).

In attempting to fit a theoretical model to numerical data some assumptions were made. The mole fraction of PI (x_{PI}) has been determined by fitting the low-temperature (LT) magnetic data to the Curie−Weiss function

(9) Renz, F. Ph.D. Thesis, Vienna University of Technology, Vienna, Austria, 1997.

$$\chi_{mol}(LT) = x_{PI}\chi_{PI} = x_{PI}C_0 g_{PI}^2[S_{PI}(S_{PI}+1)/3]/(T-\Theta_{PI}) \quad (1)$$

($C_0 = N_A\mu_0\mu_B^2/k$ comprises the fundamental physical constants in their usual meaning) assuming $S_{PI} = 5/2$ and $g_{PI} = 2.0$ for an Fe(III) center. Then the Weiss constant $\Theta_{PI} = -4.66$ K and $x_{PI} = 0.00826$ resulted on the basis of 16 lowest data-points. The fitting procedure for the whole temperature range utilizes the magnetic susceptibility function in the form

$$\chi_T = x_{HS}\chi_{HS} + x_{PI}\chi_{PI} = [(1+\langle\sigma\rangle)/2]C_0 g_{HS}^2[S_{HS}(S_{HS}+1)/3]/T + x_{PI}C_0 g_{PI}^2[S_{PI}(S_{PI}+1)/3]/(T-\Theta_{PI}) \quad (2)$$

that assumes $\chi_{LS} = 0$ for the diamagnetic $S_{LS} = 0$ state. Here, $S_{HS} = 2$ is fixed, and g_{HS} is taken as a free parameter. This equation contains a variable $\langle\sigma\rangle$, which should be iterated for each temperature, and a trial set of optimized parameters (see Experimental Section). The free parameters of the spin crossover model **B** comprise Δ_0 (the site formation energy), J (the cooperativity parameter), and $h\bar{\nu}_{HS}$ and $h\bar{\nu}_{LS}$ (the mean vibrational energies of active modes). The last two quantities collapse into a single parameter $r_{eff} > 5$ (the effective degeneracy ratio) in a more approximate model **A**.

The fitting of the whole hysteresis curve with history of the heating/cooling is far from being trivial and has not been done for spin crossover systems so far. The thermal history is encoded into the starting value of $\langle\sigma\rangle$ that enters the iteration procedure: $\langle\sigma(T_i)\rangle_{starting} = \langle\sigma(T_{i-1})\rangle_{final}$. Alternatively one can use $\langle\sigma(T_i)\rangle_{starting} = -1$ on the heating and $\langle\sigma(T_i)\rangle_{starting} = +1$ on the cooling direction, respectively.

The "simulated annealing method" and contemporary genetic algorithms have been applied in order to localize the global rather than local minima of the error functional.[10] As a result of the fitting procedure the set of parameters resulted as shown in Table 1.

The experimental susceptibility data have been processed in evaluating the "experimental" high-spin mole fraction

$$x_{HS} = \frac{(\chi_T T) - (\chi_{PI}T)x_{PI}}{(\chi_{HS}T)} \quad (3)$$

and the equilibrium constant for a unimolecular reaction LS ↔ HS

$$K = \frac{x_{HS}}{x_{LS}} = \frac{x_{HS}}{1 - x_{HS} - x_{PI}} \quad (4)$$

Having x_{PI} already determined, the evaluation of $x_{HS} = f(T)$ and $\ln K = f(1/T)$ functions would be an easy task provided that the $(\chi_{HS}T)$ product already reached its maximum value. The last assumption, although commonly met for SC systems having T_c much below the room temperature, is not fulfilled in the present case: the effective magnetic moment is still increasing at the high-temperature limit of data collection. Therefore the evaluation of the "experimental" high-spin mole fraction is disabled prior to fixing the $(\chi_{HS}T)$ limit. This can be done by assuming the fulfillment of the Curie law in the form

(10) (a) Press, V. H.; Teukolsky, S. A.; Vetteriling, W. T.; Flannery, B. P. *Numerical Recipes in Fortran*, 2nd ed.; University Press: Cambridge, 1992. (b) Goldberg, D. *Genetic Algorithms in Search, Optimization and Machine Learning*; Addison-Wesley: Reading, MA, 1989. (c) Carroll, D. L. *A Genetic Algorithm Program*, version 1.7; University of Illinois, 1998.

Table 1. Results of the Fitting the Magnetic Data[a,b]

quantity	model **A**	model **B**	model **C**
g_{HS}	1.998	1.970	2.011
Δ_0/k	2153	3414[c]	2129
J/k	473	418	454
r_{eff}	210	[5]	198
$(h\bar{\nu}_{LS})/k$		600	
$(h\bar{\nu}_{HS})/k$		399	
σ			0.0073
$R(\chi_{mol})$	0.173	0.187	0.056

[a] Values in square brackets were fixed; 160 data points were used. [b] Model **A**: Ising-like model, a constant vibrational contribution to entropy. Model **B**: vibrational contribution averaged over 15 low-energy modes. Model **C**: Gaussian decay of the optimum cooperativeness. [c] A vibronic level difference is $\Delta = \Delta_0 + (15/2)(h\bar{\nu}_{HS} - h\bar{\nu}_{LS}) = 1907$ K.

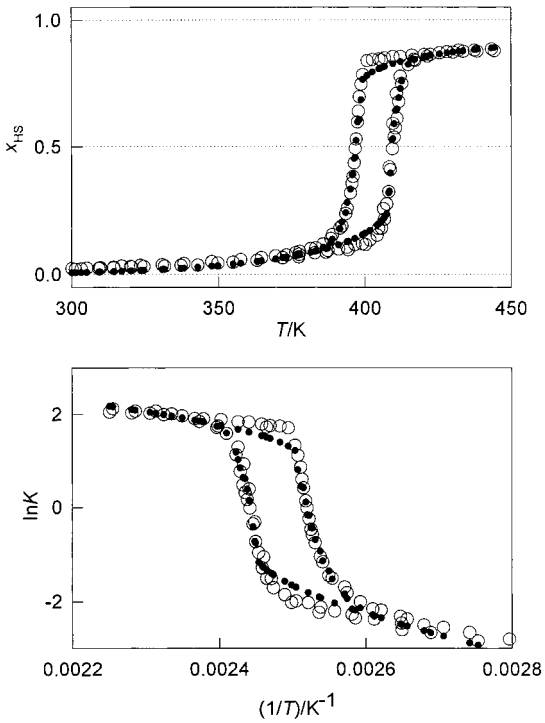

Figure 3. High-spin mole fraction (top) and van't Hoff plot (bottom) for **1**: experimental (open circles) and theoretical (full points) data with the model **C**.

$$\chi_{HS}T = C_0 g_{HS}^2[S_{HS}(S_{HS}+1)/3] \quad (5)$$

The transition temperatures are exactly read-of at $\chi_{HS} = 0.5$ (or, equivalently, at $\ln K = 0$), i.e., $T_c^{\uparrow} = 409$ and $T_c^{\downarrow} = 397$ K. The hysteresis width becomes $\Delta T = T_c^{\uparrow} - T_c^{\downarrow} = 12$ K and the center of the spin transition is at $T_c^{center} = T_c^{\uparrow} + \Delta T/2 = 403$ K (Figure 3).

The sample under investigation was cycled on DSC-600 between 100 and 450 K. In the heating regime only an endothermic peak was registered with minimum at $T_p^{\uparrow} = 414$ K and on cooling an exothermic peak with maximum at $T_p^{\downarrow} = 406$ K. No features of decomposition were registered at the highest temperature of the thermal cycling. The positions of the peaks were recovered in subsequent cycles. A more detailed inspection of the data showed, however, that the first endothermic peak (corresponding to the spin crossover) is accompanied by an endothermic satellite (which disappears either on the first cooling or the subsequent cycling). We conclude that some crystal water was liberated and not reabsorbed on the cooling. This interpretation is supported by the VT-IR data.

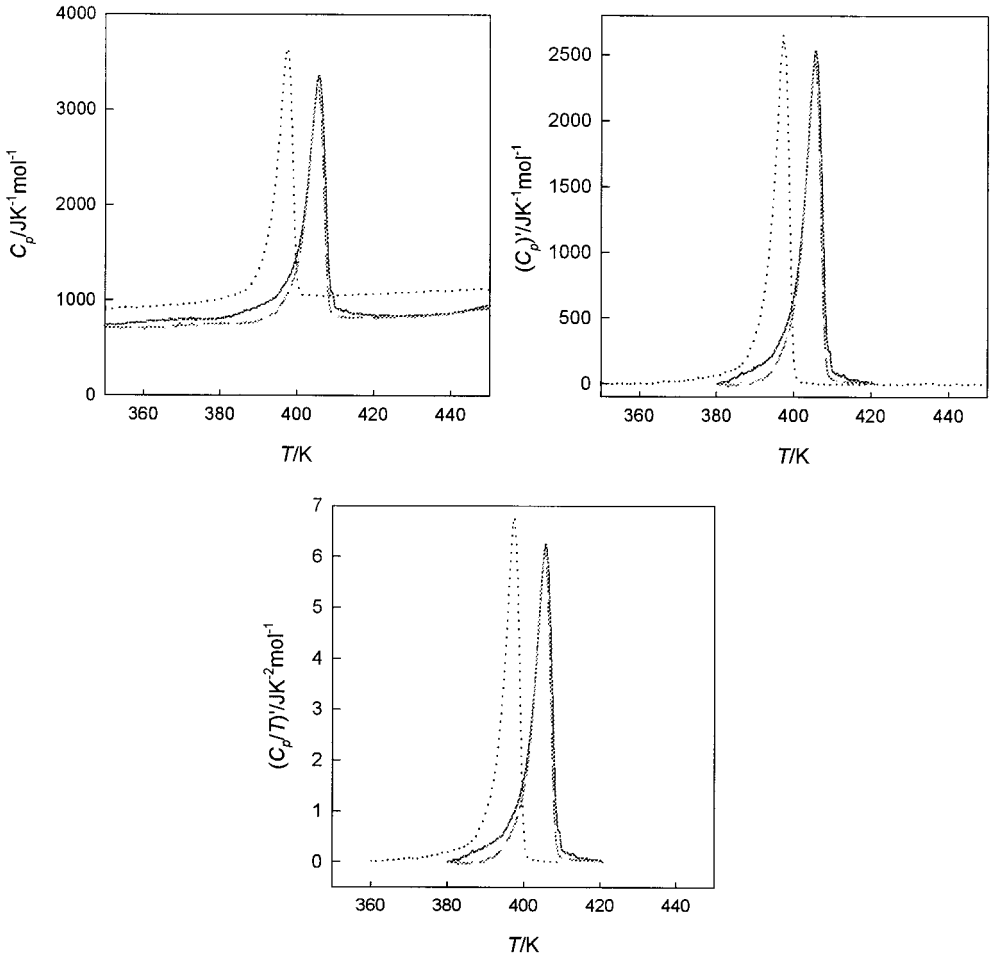

Figure 4. Left: measured temperature dependence of the heat capacity for **1**. Right: an under-integral enthalpic function (C'_p vs T). Center: an under-integral entropic function ($(C_p/T)'$ vs T). Solid: microcrystalline sample **c** on the first cooling. Dashed: microcrystalline sample **c** on the second cooling. Dotted: powder sample **b** on the first cooling.

For a quantitative treatment the heat flow was scanned on the DSC-2 and DSC-7 apparatus in the higher temperature window (the broad satellite owing to some crystal water disappeared on the further thermal cycling). The onset temperatures on heating and cooling were read-of using the second cycle data, according to the literature recommendation.[11] They appear approximately at the same position $T_c = 403$ K on the heating and the cooling, respectively.

The heat flow from the first cooling and independent measurements of a free container and a calibration standard allowed the evaluation of the molar heat capacity. As displayed in Figure 4, the spin transition is indicated by a well-developed λ-shaped peak either on the C_p vs T or (C_p/T) vs T function. After the subtraction of the underlying Debye part due to molecular vibrations, the numerical integration gave the enthalpy, $\Delta H = (17.4 \pm 1.0)$ kJ mol^{-1}, and the entropy of the spin transition, $\Delta S = (43.1 \pm 1.0)$ J K^{-1} mol^{-1}, respectively.

Far-infrared spectra exhibit two patterns characteristic for the spin crossover systems (Figure 5). The band at $\tilde{\nu}_{HS}$ 270−310 cm^{-1} is characteristic for the high-spin centers and it appears on sample heating. The area at $\tilde{\nu}_{LS} = 415-445$ cm^{-1} is characteristic for the low-spin centers and it disappears on heating. An unusual feature of this region is that two sub-bands ($\tilde{\nu}_{LS1} = 415-430$ cm^{-1} and $\tilde{\nu}_{LS2} = 430-445$ cm^{-1}) exist; they behave differently on the sample heating.

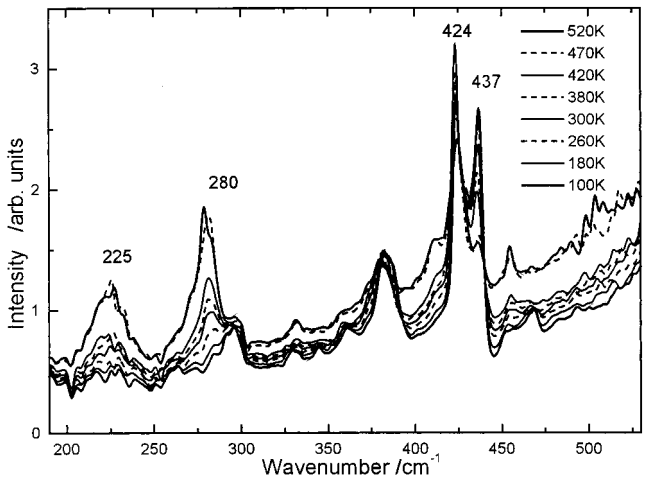

Figure 5. FT-IR spectra of **1** on heating.

The band areas have been processed in calculating the mole fractions for HS, LS1, and LS2 centers

$$x = \frac{A_T - A_{min}}{A_{max} - A_{min}} \quad (6)$$

where A_{min} is the minimum band area on thermal treatment (for the LS band at the highest temperature and for the HS band at the lowest temperature); A_{max} is the maximum band area on thermal treatment; and A_T is the band area at temperature T.

(11) Höhne, G.; Hemminger, W.; Flammersheim, H.-J. *Differential Scanning Calorimetry*; Springer: Berlin, 1996.

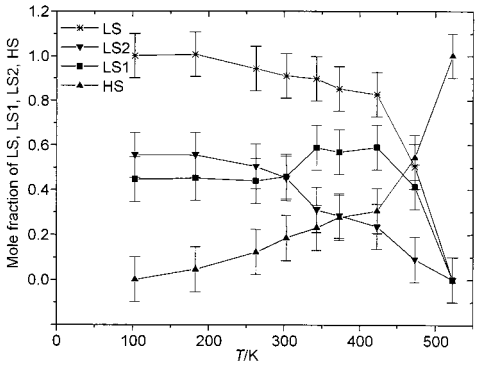

Figure 6. Temperature variation of the mole fraction for the LS and HS vibrations for **1** on heating direction (the connecting lines serve only as a guide for the eyes).

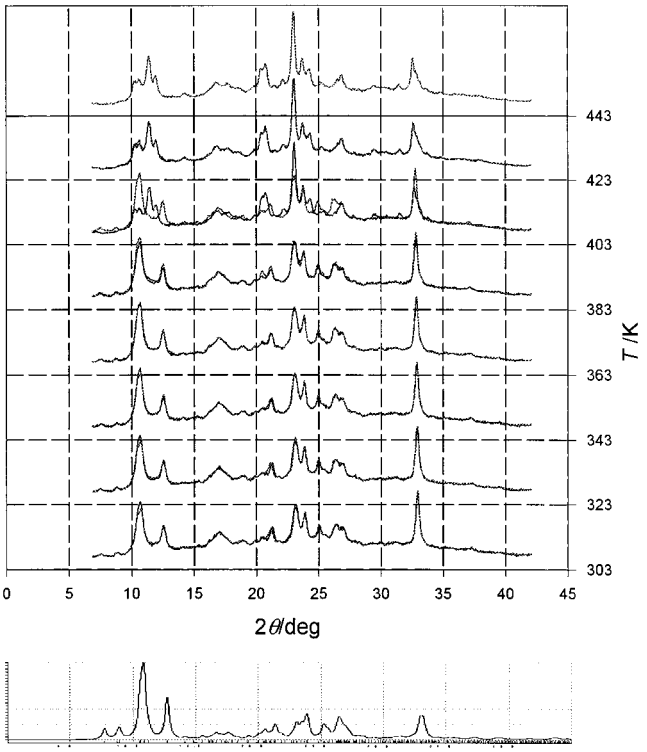

Figure 7. Top: evolution of the powder diffraction pattern for **1** on temperature cycling (second cycle). Individual pattern shown for heating $T^{\uparrow}$ = 303, 323, 343, 363, 383, 403, 423, 443 K and for cooling $T^{\downarrow}$ = 423, 403, 383, 363, 343, 323, 303 K (these are added at the same place as those for $T^{\uparrow}$). Bottom: theoretical pattern based on the room-temperature X-ray structure. (The reader is recommended to watch the figure at a very sharp angle for a better impression.)

Their temperature dependence is shown in Figure 6. The higher frequency band LS2 shows a smooth decrease of its area whereas the lower-frequency band LS1 tends to increase its area above 300 K, but above 430 K an abrupt decrease is observed. The sum of these areas is nearly constant: $A_{HS} + A_{LS1} + A_{LS2} \approx$ constant. The bands LS1 and LS2 could correspond to two nonequivalent low-spin sites.

The Mössbauer spectra between 10 and 293 K show only a low-spin doublet (small quadrupole splitting) and no evidence for an eventual differentiation between LS1 and LS2 centers.

The X-ray powder diffraction patterns were scanned in three cycles, starting with T_{min} = 303 K, until T_{max} = 443 K, and back, the temperature increment being δT = 20 K (Figure 7). The diffraction patterns alter at $T^{\uparrow}$ = 423 K on heating and they return back perfectly at $T^{\downarrow}$ = 383 K on cooling. Only the first cycle on heating is slightly different probably due to liberation of some crystal water.

Also the theoretical powder diffraction patterns, calculated on the basis of the room-temperature X-ray structure, are displayed in Figure 7.

Discussion

Sample Properties. The freshly prepared sample, $[Fe(bzimpy)_2](ClO_4)_2 \cdot xH_2O$, contains some amount of water. The crystal structure confirms $x = 0.25$ but this amount is not ultimate for the powder samples prepared by a fast precipitation.[8]

The O−H stretching vibrations in IR spectra disappear on the first heating and the DSC signal shows an endothermic peak at 430 K. A rather small mass-loss on thermogravimetry evidences $x < 1$.

The sample exhibits some paramagnetic impurity which was assigned to the Fe(III) centers on the basis of ESR spectra.

None of the above factors manifests itself in the key features of the spin crossover. The liberation of some crystal water does not influence the spin crossover, which remains perfectly reversible as evidenced from magnetic data (2 cycles), DSC (2 cycles), VT-IR data (2 cycles), and VT-powder diffraction data (3 cycles). The paramagnetic impurity ($x_{PI} = 0.008$) can only influence the background-paramagnetism and finally the recorded magnetic susceptibility and/or the value of the effective magnetic moment at low temperature.

Solid samples prepared by the same recipe (possessing correct C, H, N content) may exhibit a color-variance (violet, dark-violet, black-violet). This may be due to a different size of solid particles. Ethanol solutions of these samples have the same vinered color and identical electron spectrum. Aging of the sample manifests itself in the color alteration to pale-violet, probably due to the surface oxidation. A one year-old sample can possess more than 5% of Fe(III).

Magnetic Data. The first magnetic (SQUID) investigation on **1** yielded a continuous increase of the effective magnetic moment on heating with $\mu_{eff} = 3.0\ \mu_B$ at 340 K.[12] Later investigation (Evans-NMR method) in solution evidenced a spin crossover behavior influenced by the solvent used.[13] Further investigation of the solid sample (Faraday balance) confirmed the spin crossover, although incomplete at room temperature as well as at 410 K: $\mu_{eff} = 3.55\ \mu_B$ at 410 K.[8] The new aspect of the present investigation is that **1** exhibits an abrupt spin crossover above 400 K with a number of unique properties: $T_c^{\uparrow} = 409$ K, $T_c^{\downarrow} = 397$ K, and the hysteresis width of $\Delta T = 12$ K.

The existence of the hysteresis is conditioned by a considerable value of the cooperativity parameter J and it can occur only when $J/k > T_c$. Thus an important conclusion follows directly from experimental data: the lower limit of the cooperativity parameter is $J/k > 403$ K in the compound under investigation. One should accept such a high value despite the fact that the Fe(II) centers are 10 Å apart from each other.[8] It is obvious that the "through-space" magnetic dipole−dipole interactions are incapable of such a strength.

Since our system exhibits a strong cooperativeness, comparable to T_c, then distribution factors may adopt a great importance: domains of a different nuclearity can be formed and a cooperativeness of the spin crossover altered. It has been already reported that the graining of the powder samples could

(12) Addison, A. W.; Burman, S.; Wahlgrem, C. G.; Rajan, O. A.; Rowe, T. M.; Sinn, E. *J. Chem. Soc., Dalton Trans.* **1987**, 2621.
(13) Linert, W.; Konecny, M.; Renz, F. *J. Chem. Soc., Dalton Trans*. **1994**, 1523.

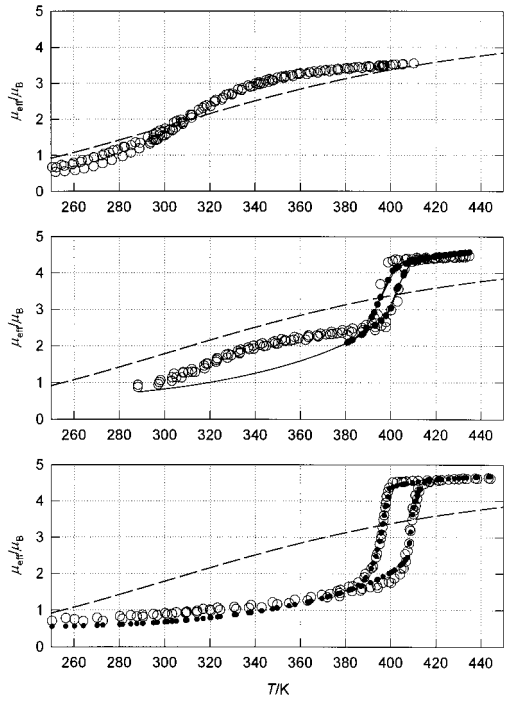

Figure 8. Effective magnetic moment (open symbols) for samples of **1** with different history (top, sample **a**; center, sample **b**; bottom, sample **c**). Full points: fitted data using the theoretical model **C**. Solid line (center): predicted. Dashed line: a theoretical curve in the absence of the cooperativeness.

reduce the steepness of the spin transition so that the onset of the transition is observed at a lower temperature.[1f] A recent report confirms that the profile of the spin crossover for a single-crystal is much steeper than that of a powder-sample.[6a]

The above factors could rationalize the discrepancies in the published magnetic data for **1** along with Figure 8 showing our data collection for three samples of a different history.

The first data set (**a**, half-year old sample, fine powder, pale-violet) exhibits the broadest distribution owing to which the onset temperature of the spin crossover becomes evident at 250 K. We had no motivation to continue with heating above 400 K that time.[8] We reported about a "pronounced hysteresis between 220 and 414 K" which, with the present knowledge, would be better termed the "different path on heating and cooling".

The second data set (**b**, fresh sample, fine powder, dark violet) scanned until 450 K shows a reduced distribution: the onset temperature of the spin crossover is about 300 K. The system behaves like a two-step spin crossover: the first step being rather continuous and the second one very sharp with $T_c^{\uparrow} = 405$ K, $T_c^{\downarrow} = 397$ K, and $\Delta T = 8$ K.[14]

The third data set (**c**, fresh sample, microcrystalline, black-violet) shows a suppressed distribution and only one sharp step (present investigation). The dashed line in Figure 8 represents a pure Boltzmann equilibrium when the cooperativeness is absent (like in solutions). The full points in Figure 8 result from a theoretical analysis and will be discussed later.

Calorimetry. Our calorimetric readings of the characteristic temperatures for the sample **c** are collected in Table 2. The determined value of $\Delta H = 17.4$ kJ mol^{-1} lies at the higher limit of the experimental data published for similar compounds.[1] The entropy change $\Delta S = 43.1$ J K^{-1} mol^{-1} lies just in the center

(14) Lemercier, G.; Varelst, M.; Bousseksou, A.; Varret, F.; Tuchagues, J.-P. In *Magnetism: A Supramolecular Function*; Kahn, O., Ed.; Kluver: Dordrecht, 1996.

Table 2. Survey of Quantitative Data for 1 (Fresh, Microcrystalline Sample **c**)[a]

quantity	magnetic susceptibility	DSC calorimetry	IR spectra	theoretical model **A**	theoretical model **B**
$T^{\uparrow}$/K	$T_c^{\uparrow} = 409$	$T_p^{\uparrow} = 414$		$T_c^{\uparrow} = 409$	$T_c^{\uparrow} = 409$
$T^{\downarrow}$/K	$T_c^{\downarrow} = 397$	$T_p^{\downarrow} = 406$		$T_c^{\downarrow} = 397$	$T_c^{\downarrow} = 397$
ΔH/kJ mol^{-1}		17.4		17.9	
ΔS/J K^{-1} mol^{-1}		43.1		44.4	
$(\Delta H/\Delta S)$/K		404		403	
$\tilde{\nu}_{LS}$/cm^{-1}			424, 437		417
$\tilde{\nu}_{HS}$/cm^{-1}			225, 280		277

[a] T_p, peak maximum value; T_c, passage through the critical value $x_{HS} = 0.5$.

of the interval of published data and it is very typical for the iron(II) hexacoordinate spin crossover systems. A good test of consistency of these experimental determinations is the ratio $T_c^{\text{predicted}} \approx \Delta H/\Delta S = 404$ K.

For the powdered sample **b** we found the following: $T_p^{\uparrow} = 406$ K, $T_p^{\downarrow} = 397$ K, enthalpy $\Delta H = 15.4$ kJ mol^{-1}, and the entropy of the spin transition, $\Delta S = 40.0$ J K^{-1} mol^{-1}, respectively.

Thermodynamics vs Theoretical Models. The experimental thermodynamic quantities that directly relate to the spin transition cover ΔH, ΔS, and T_c (in the case of hysteresis $T_c^{\uparrow}$ and $T_c^{\downarrow}$). In the absence of cooperativity, the high-spin mole fraction is a simple function of the enthalpy and the entropy of the transition, i.e.,

$$x_{HS} = 1/\{1+\exp[(\Delta H/R)(1/T - 1/T_c)]\} \qquad (7)$$

where $T_c = \Delta H/\Delta S$ assumes temperature independent enthalpic and entropic contributions. For the $\{Fe^{II}N_6\}$ chromophore the entropic contribution is rather constant, $\Delta S \approx 40$ J K^{-1} mol^{-1}, as a result of electronic and low-frequency vibrational contributions. Then the necessary conditions for having the spin transition above room temperature is to raise the enthalpic contribution, i.e., to disfavor the spin transition.

There is a number of contributions to the overall ΔH in the solid state: the nature of the metal-containing unit, quality of counterions, their packing, and solvents embodied in the crystal lattice. All these factors can tune the ΔH and consequently T_c expressively.[14] One of the dominant contributions is given by the energy difference in the adiabatic potential surfaces: $\Delta H^{el} \approx \Delta E^{el} = E_{HS} - E_{LS}$.

The bidentate ligands with a fixed donor atom separation (like phenanthroline, bipyridine, pybzim, etc.) are somehow disfavored on the spin crossover since not all six vertexes can accommodate the required increase in the metal−ligand bond lengths by ca. 15%. For this reason the enthalpy of the transition spans the value of ca. $\Delta H \approx 3-6$ kJ mol^{-1} and the transition temperature ranges as $T_c = 100-200$ K. For example, in the complex $[Fe(pybzim)_3](ClO_4)_2 \cdot H_2O$, where pybzim = 2,2′-pyridine-benzimidazol, the presence of three *rigid* bidentate ligands results in the values of $\Delta H = 3.3$ kJ mol^{-1}, $\Delta S = 23.2$ J K^{-1} mol^{-1}, and $T_c = 142$ K.[15]

The tridentate ligands with a fixed donor atom separation (like tris(pyridine), tris(imidazole), and bis(benzimidazole)-pyridine) represent much more rigid units which under the spin

(15) (a) Boča, R.; Boča, M.; Jaroščiak, R.; Vrbová, M. *J. Mol. Cryst. Liq. Cryst.* **1999**, *335*, 551. (b) Boča, R.; Baran, P.; Dlháň, L'.; Sima, J.; Wiesinger, G.; Renz, F.; El-Ayaan, U.; Linert, W. *Polyhedron* **1997**, *16*, 47. (c) Boča, R.; Vrbová, M.; Werner, R.; Haase, W. *Chem. Phys. Lett.* **2000**, *382*, 188.

crossover increase the energy gap considerably ΔE^{el}. Thus the substitution of the bidentate for *rigid* tridentate heterocyclic ligands can systematically raise the temperature of the spin transition toward or even above the room temperature. This was really observed for the system under study where the $\Delta H = 17.4$ kJ mol^{-1} and $\Delta S = 43.1$ J K^{-1} mol^{-1} values predetermine the transition temperature $T_c = 403$ K. However, counterions bring a considerable contribution as well: $T_c = 330$ for [Fe(bzimpy)$_2$](BPh$_4$)$_2$·4H$_2$O, $T_c = 403$ K for [Fe(bzimpy)$_2$](ClO$_4$)$_2$·0.25H$_2$O, and T_c is not reached for [Fe(bzimpy)$_2$]SO$_4$·2H$_2$O until 480 K.

The involvement of a cooperativity parameter (e.g., the "interaction" constant among LS−HS entities, like $E_{inter} = \gamma x_{HS}(1-x_{HS})$ in the regular solution model)[16] makes the transition curve more steep when compared to a simple Boltzmann distribution. As far as the van't Hoff plot obeys a nonlinearity around $\ln K = 0$, the cooperativity parameter can be deduced on the basis of an appropriate theoretical model. When the cooperativity parameter overreaches its critical value $\gamma/2 > RT_c$, the hysteresis can occur.

The Ising-like model used for the quantitative analysis of magnetic data has several advantages: (i) in its version **A** it is equivalent to the regular solution model through the correspondence $\gamma/2 \leftrightarrow N_A J$; (ii) it allows an elegant involvement of the vibrational partition function into the model **B**; (iii) it has been extended to a two step process or to binuclear systems. However, the existence of domains and distribution are not covered by this approach. The original version of the domain model, on the contrary, violates in predicting the hysteresis unless different domain sizes for LS and HS states are assumed.

A positive feature of the theoretical model **A** is its capability of the reproduction of the thermodynamic functions: $\Delta H^{magnetic} = N_A\Delta_0 = 17.9$ kJ mol^{-1} and $\Delta S^{magnetic} = R \ln r_{eff} = 44.4$ J K^{-1} mol^{-1} in a satisfactory agreement with the experimental calorimetric determination (Table 2). In the model **B** the entropy part is temperature-dependent owing to the thermal population of vibrational states. The main advantage of the improved model **B** is that the degeneracy ratio r_{eff} need not be considered as an "internal parameter" of the theory anymore. It is simply substituted for the transparent physical quantities: the true electronic degeneracy ratio $r_{el} = 5$ and the mean vibrational energies. The last set can be monitored by IR or Raman spectroscopy.[17] The ratio $\bar{\nu}_{LS}/\bar{\nu}_{HS} = 1.5$ is probably a bit higher than generally accepted (1.3) but this has a little effect to the fitting procedure (this can alter only the low-temperature part of the data which, in our case, are overlapped by the background signal of PI).

On the basis of Table 2, one can conclude that the theoretical models are fully consistent with information withdrawn from magnetic susceptibility data, calorimetric data, and the IR spectra.

The main success of the theoretical model **C**, which accounts for the distribution of the cooperativity parameter, is its capability of predicting the slope of the walls of the hysteresis loop. We assume that with the model **C** a lot of nonideal spin crossover behavior could be explained, at least a different profile of the hysteresis path for powder samples prepared by a different rate of precipitation.[6] Our hypothesis of the Gaussian decay of the cooperativeness should be viewed as a first, probably not ideal, trial; other distribution curves could be easily incorporated into the model **C**.[20,21]

Finally we recovered the experimental data set on Figure 8b (fine-powder sample) by the set of parameters $g_{HS} = 2.037$, $\Delta_0/k = 2053$, $r_{eff} = 171.7$, $J/k = 489$ K, and $\sigma = 0.114$).

In summary, the microscopic spin-crossover parameters adopt the following meaning: (i) the site formation energy Δ_0 relates to the molar enthalpy of the spin transition through the relationship $\Delta H = R(\Delta_0/k)$; (ii) the effective degeneracy ratio determines the molar entropy of the transition $\Delta S = R \ln r_{eff}$; (iii) the ratio $\Delta H/\Delta S = T_c$ gives the temperature of the spin transition (the center of the hysteresis); (iv) the cooperativity parameter is associated with the nonlinearity of the van't Hoff plot around T_c and it determines the hysteresis width when $T_c < n(J/k)$; and (v) the distribution parameters n and σ are associated with the steepness of the walls of the hysteresis loop. The role of the cooperativity parameter (J or γ) lies in a damping that reduces the Boltzmann population of the HS below T_c. Above T_c it becomes an accelerating force of the high-spin fraction.

Notice, a uniform rescaling of $\Delta H = n(\Delta H')$ and $\Delta S = n(\Delta S')$ does not affect the transition temperature $T_c = \Delta H/\Delta S = \Delta H'/\Delta S'$. Analogously, rescaling of the cooperativeness $J = nJ'$ does not affect the hysteresis width: $\Delta T \approx (J/k) - T_c \approx n(J'/k) - \Delta H'/\Delta S'$. Now when n decays according to some distribution, T_c remains conserved but ΔT decreases from case to case. In a statistical average one can see angled walls of the hysteresis loop (and other consequences, like a decrease of the hysteresis width, decrease of the degree of conversion at high temperature, and increase of the low-spin background at low temperatures).

Structure vs Cooperativeness. On the basis of the magnetic data, the room-temperature structure is assigned to the LS state. The temperature cycling of the powder diffraction patterns (PDP) shows that the spin crossover at $T_c = 403$ K is associated with some structural changes. This, however, becomes perfectly reversible in the second and the third cycle when the crystal water is not present anymore. On return to room temperature the PDP match well the theoretical patterns calculated on the basis of the room-temperature X-ray structure (the presence of the crystal water is irrelevant for the calculated PDP). The improved reproducibility in subsequent cycles is not a big surprise; similar effect has been reported elsewhere.[3a]

Figure 9 brings some structural details at room temperature (not presented so far): each iron(II) center has six nearest neighbors at a distance of about Fe−Fe′ = 10 Å (9.79, 9.88, 10.04, 10.35, 10.40, 10.54 Å) and there are nine more neighbors within the radius of 15 Å (12.28, 12.54(2×), 13.71, 13.78, 13.81(2×), 14.50(2×) Å). It can be seen that the planes of the ligand are perpendicular within the complex and packed perfectly in a parallel manner between different units. Despite the fact that some hydrogen bonds have been identified within the structure we assume that the hydrogen bonds do not transmit the Fe(II)-Fe(II)′ communication. A perfect π-stacking of the phenyl rings from different units exists; the C−C′ contacts

(16) Slichter, C. P.; Drickamer, H. G. *J. Chem. Phys.* **1972**, *56*, 2142.
(17) Bousseksou, A.; McGarvey, J. J.; Varret, F.; Real, J. A.; Tuchagues, J.-P.; Dennis, A. C.; Boillot, M. L. *Chem. Phys. Lett.* **2000**, *318*, 409.
(18) Addison, A. W.; Burke, P. J. *J. Heterocycl. Chem.* **1983**, 1481.
(19) (a) Bousseksou, A.; Nasser, J.; Linares, J.; Boukheddaden, K.; Varret, F. *J. Phys. I* **1992**, *2*, 138. (b) Bousseksou, A.; Varret, F.; Nasser, J. *J. Phys. I* **1993**, *3*, 1463. (c) Bousseksou, A.; Constant-Machado, H.; Varret, F. *J. Phys. I* **1995**, *5*, 747. (d) Lemercier, G.; Bousseksou, A.; Seigeuric, S.; Varret, F.; Tuchagues, J.-P. *Chem. Phys. Lett.* **1994**, *226*, 289. (e) Linares, J.; Spiering, H.; Varret, F. *Eur. J. Phys. B* **1999**, *10*, 271. (f) Bousseksou, A.; Salmon, L.; Varret, F.; Tuchagues, J.-P. *Chem. Phys. Lett.* **1998**, *282*, 209. (g) Bousseksou, A.; Varelst, M.; Constant-Machado, H.; Lemercier, G.; Tuchagues, J.-P.; Varret, F. *Inorg. Chem.* **1996**, *35*, 110.
(20) Cantin, C.; Kliava, J.; Marbeuf, A.; Mikailitchenko, D. *Eur. Phys. J.* **1999**, *B12*, 525.
(21) Constant-Machado, H.; Stancu, A.; Linares, J.; Varret, F. *IEEE Trans. Magnet.* **1998**, *34*, 2213.

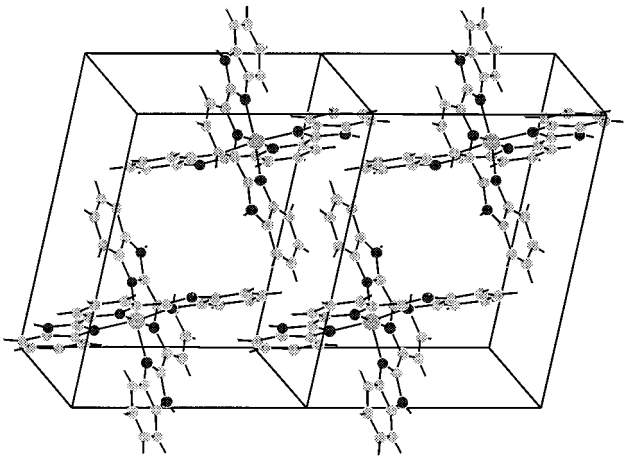

Figure 9. A view to the unit cell content of **1** duplicated along the *a*-direction. The perchlorate groups and the oxygen atom were omitted for clarity.

varying between 3.60 and 3.99 Å (3.78, 3.72, 3.80, 3.94, 3.99, 3.88, 4.39, 4.13, 3.71, 3.61, 3.88, 4.24 Å).

Taking into the fact that the steepness of the spin-crossover is driven by the cooperativity parameter, we would like to address a question about its physical nature. Similar attempts have appeared in the literature trying to correlate the cooperativeness and the structure features. Noticeable is the fact that in systems with high cooperativity some π-stacking of aromatic rings exists.[6] The physical mechanism associated with it remains unmodeled so far.

In conclusion, the spin crossover system, $[Fe(bzimpy)_2](ClO_4)_2 \cdot 0.25H_2O$, exhibits an abrupt low-spin to high-spin transition at $T_c = 403$ K. Liberation of a fractional amount of water does not affect the spin crossover: the system is perfectly reversible with a hysteresis width of $\Delta T = 12$ K. The existence of the hysteresis at such high temperature determines that the lowest limit of the solid-state cooperativity parameter is $J/k > 403$ K despite long iron(II) separations (10 Å). The high cooperativeness has been assigned to a perfect π-stacking of the benzimidazole rings in the crystal lattice at a distance as short as 3.6 Å.

The variable-temperature IR data and the heat capacity measurements match well the magnetic data. The enthalpy of the transition is $\Delta H = 17$ kJ mol^{-1}, and the entropy of the spin transition possesses a considerable contribution from the molecular vibrations ($\Delta S = 43$ J K^{-1} mol^{-1}). A theoretical model has been applied in fitting the magnetic data along the whole hysteresis path. A statistical distribution of the cooperativity parameter led to the feature that angled walls of the hysteresis loop are well reproduced.

Experimental Section

Preparation. The ligand bzimpy and its complex of $[Fe(bzimpy)_2](ClO_4)_2 \cdot xH_2O$ were prepared by the procedures described elsewhere.[18,8] The elemental analysis (within the error bars) confirmed the C, H, N content. As the sample could be sensitive to oxygen, all manipulations were done under nitrogen atmosphere.

CAUTION. On heating, the sample can explode at temperatures above 470 K owing to the presence of perchlorate. Heating until 470 K is safe.

Magnetic Susceptibility Measurements. The mass magnetic susceptibility has been measured with Faraday-type balances at the applied field $B = 1.4$ T. The sample under an applied vacuum was cycled as follows: 309−5−320−289−443−373−421−317 K. Each data point has been assigned with a flag indicating the temperature history (heating and/or cooling). During the spin crossover the heating/cooling rate was much smaller than 1 K/min. The correction for an underlying diamagnetism has been performed with the set of Pascal constants: $\chi_{dia} = -5.834 \times 10^{-9}$ m^3 mol^{-1}.[1h] The corrected molar magnetic susceptibility has been converted to the effective magnetic moment $\mu_{eff}/\mu_B = 798(\chi'_{mol}T)^{1/2}$; SI units are employed.

Infrared Spectroscopy. The FT IR-2000 apparatus (Perkin-Elmer) has been used for variable temperature experiments between 100 and 520 K. Temperature was controlled using a thermocouple (Grasby/Specac) and kept constant within ±1 K. A resolution of 1 cm^{-1} using a mirror velocity of 2.0 mm s^{-1} was used and the band positions could be reproduced within ±0.3 cm^{-1}. The sample was mounted as a CsI pellet and 1000 scans were taken per spectrum.

Powder Diffraction. The STOE-STADIP powder diffractometer was used with programmed temperature regime: temperature was kept constant within ±0.1 K. The diffraction patterns using the Co Kα radiation ($\lambda = 1.78892$ Å) were scanned within the interval $5 \le 2\vartheta \le 45$ deg.

DSC Calorimetry. The DSC-600 apparatus (Linkam) has been used to scan the heat flow. Several temperature cycles were applied: 100−450−100 K, 300−450−300 K.

The DSC-2 and DSC-7 apparatus (Perkin-Elmer) has been used to record the heat flow of the sample (9.0 mg), free sample holder (aluminum pan), and the sapphire filled container (scan rate, 5 or 10 deg/min; scan frequency, 1 s). The recorded heat flows were processed by the well-known procedure to obtain the mass heat capacity of the sample: (i) all isothermal edges were linearly transformed to the same origin; (ii) the sample holder signal was subtracted from the sapphire and sample heat flows; (iii) the net sapphire heat flow and tabulated sapphire heat capacity was used to calibrate the net sample heat flow into the heat capacity of the sample.[11] The procedure assumes the constant waiting periods before and after the heating and/or cooling and the constant temperature change. A temperature cycle 320−450−320 K was applied twice.

The Debye part due to molecular vibrations has been subtracted from the heat capacity curve assuming that the functions $C_p = aT^3$ and $C_p/T = bT^2$ hold true. Thus a few data below the onset temperature were used to determine the constants a_{LS} (b_{LS}) and a few data above the transition to fit the constants a_{HS} (b_{HS}). Then the heat capacity was corrected for the underlying Debye part, which is different below and above the peak maximum T_p, hence

$$C'_p = C_p - a_{LS}T^3, \text{[for } T < T_p\text{]} \tag{8a}$$

$$C''_p = C_p - a_{HS}T^3, \text{[for } T > T_p\text{]} \tag{8b}$$

and

$$(C_p/T)' = (C_p/T) - b_{LS}T^2, \text{[for } T < T_p\text{]} \tag{9a}$$

$$(C_p/T)'' = (C_p/T) - b_{HS}T^2, \text{[for } T > T_p\text{]} \tag{9b}$$

Finally the enthalpy and the entropy of the transition were evaluated by a numerical integration

$$\Delta H = \int_{T_{min}}^{T_p} C'_p dT + \int_{T_p}^{T_{max}} C''_p dT \tag{10}$$

$$\Delta S = \int_{T_{min}}^{T_p} (C_p/T)' dT + \int_{T_p}^{T_{max}} (C_p/T)'' dT \tag{11}$$

Theoretical Model. Among a variety of spin crossover model the Ising-like model has been utilized in the numerical analysis. It is based on the Hamiltonian

$$\hat{H} = (\Delta_0/2)\hat{\sigma} - J\langle\sigma\rangle\hat{\sigma} \tag{12}$$

that accounts for the site formation energy Δ_0, and the spin−spin interaction taken in the mean-field approximation. Here the fictitious spin $\hat{\sigma}$ adopts values of −1 for low-spin and +1 for the high-spin state, respectively. Its thermal average, $\langle\sigma\rangle$, is directly related to the high-spin mole fraction: $x_{HS} + (1 + \langle\sigma\rangle)/2$. The formal spin operators are

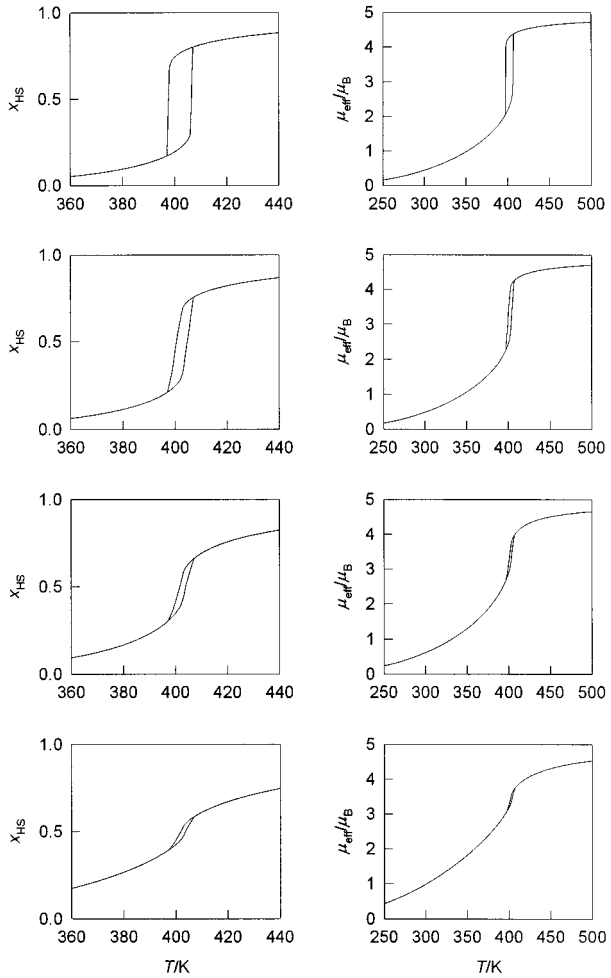

Figure 10. Modeling of the spin crossover with a Gaussian distribution of the cooperativeness for $\sigma = 0.00001$ (top), 0.01, 0.1, and 1.0 (bottom). The other spin-crossover parameters were fixed ($\Delta_0/k = 2144$ K, $J/k = 452$ K, $r_{eff} = 205$; $g_{HS} = 2.0$); $0 \le n_i \le n_{opt} = n_{max} = 1$.

not to be confused with the true (physical) spin and, analogously, the interaction constants do not have the meaning of an exchange coupling (with the sign convention in the Hamiltonian, $J > 0$ describes the "ferromagnetic"-like or "cooperative" interaction that prefers centers of like spin).

The essential features of such a model are well-described elsewhere.[19,1h] Consequently an implicit equation is to be obeyed

$$\langle\sigma\rangle = \frac{-1 + f(\langle\sigma\rangle)}{1 + f(\langle\sigma\rangle)} \tag{13}$$

In the simplest version (model **A**) there is

$$f^{(A)} = r_{eff} \exp[-(\Delta_0 - 2J\langle\sigma\rangle)/kT] \tag{14}$$

and the effective degeneracy ratio, $r_{eff} = r_{el}r_{vib} > 5$, accounts for the constant electronic as well as vibrational contribution. In a more advanced treatment (model **B**) the vibrational contribution is averaged over m-active modes ($m = 15$ for a hexacoordinate complex) and thus

$$f^{(B)} = \left\{ r_{el}\left[\frac{1 - \exp(h\bar{\nu}_{LS}/kT)}{1 - \exp(h\bar{n}_{HS}/kT)}\right]^m \right\} \exp\{-[m(h\bar{\nu}_{HS} - h\bar{\nu}_{LS})/2 + \Delta_0 - 2J\langle\sigma\rangle]/kT\} \tag{15}$$

(The nonconstant vibrational contribution dominates at low temperatures and modifies the linearity of the van't Hoff plot.) During the fitting procedure eq 13 needs to be iterated for each temperature and a trial set of parameters Δ_0, J, r_{eff}, and/or $h\bar{\nu}_{HS}$ and $h\bar{\nu}_{LS}$.

The main difference between models **B** and **A** here is that instead of $r_{eff} > 5$ as a free parameter one has $r_{el} = 5$ and a couple of the averaged vibrational energies.

The need of accounting for some parameter distribution stimulated us to modify the model **A** to that which accounts for a nonuniform intracenter interaction (hereafter **C**). We were motivated by the combination of the domain and the regular solution models.[20] In the domain model the LS and HS centers are not distributed in a random fashion within the assembly, but form domains of like spin. When n is the number of molecules per domain, then the minimum of the Gibbs energy yields the equation[20]

$$\ln K = \ln\frac{x_{HS}}{1 - x_{HS}} = -[\Delta H - T\Delta S + \gamma(1 - 2x_{HS})]n/RT \tag{16}$$

Consequently the functional factor in eq 13 will be modified to the form

$$f^{(C)} = \exp\{-[\Delta H - T\Delta S - \gamma(2x_{HS} - 1)]n/RT\} = \exp\{-[\Delta_0 - kT\ln r_{eff} - 2J\langle\sigma\rangle n]n/kT\} \tag{17}$$

This seems be a little modification with respect to eq 14 since the number n cannot be fitted independently of ΔH, ΔS, γ (molar-set parameters) or Δ_0, r_{eff}, J (molecule-set parameters). Thus, taking $n = 1$, one has the same situation as in the model **A**. Now in the domain model one parameter (say ΔH) needs to be fixed through experimental determination, and then the rest (ΔS, γ, n_{opt}) can be evaluated.

In our model **C** we formally take $n_{opt} = 1$ as the highest limit, optimum in the single crystal or particles of a sufficient size. Under the "distribution" we understand the existence of particles of lower than the optimum domain size in the real powder material. In our hypothesis the optimum parameter J decays along with the Gaussian distribution, i.e., the individual weights are

$$w_i \approx \exp[-(n_i - n_{opt})^2/\sigma] \tag{18}$$

Here the half-width parameter σ is considered as a quantity that characterizes the imperfect (powder) sample. Its value is very low ($\sigma < 0.01$) for an almost perfect sample. Now the distribution is accounted for through the average

$$x_{HS} = [\sum_{i=1}^{M} w_i \cdot x_{HS}(n_i)]/[\sum_{i=1}^{M} w_i] \tag{19}$$

where M is the number of grid-points between n_{min} and n_{max}. The consequences of the model **C** are well visible in Figure 10. With $\sigma = 0.00001$ there is an abrupt spin transition with steep walls of the hysteresis loop. On σ increase the following occur: (i) the hysteresis width decreases; (ii) the walls of the hysteresis loop become less steep; (iii) the degree of conversion at high temperature as lowered; (iv) the low-spin background at low temperature is higher.

The performance of the fitting procedure with the model **C** proceeds in several nested loops: (i) the first loop handles with free parameters to be optimized; (ii) the temperature loop is opened for experimental data-points; (iii) the J-distribution loop is opened for the grid-points; (iv) the implicit equation for the high-spin mole fraction (13) is iterated.

Acknowledgment. We are pleased to acknowledge the support of the bilateral Slovak-Germany program, Project SLA-005-97, and the Slovak Grant Agency, Project 1/6083/99. The authors are thankful to Prof. F. Varret (Versailles, France) for his interest in the work and help with discussion.

IC000807S